Inorganic Micelles (Hydrophilic Core@Amphiprotic Shell) for Multiple Applications

Md. Shahinul Islam, Won San Choi, Sun Ha Kim, Oc Hee Han, and Ha-Jin Lee**

A facile approach for synthesizing superhydrophobic hollow silica micelles (SHSMs) with hydrophilic cores and amphiprotic (superhydrophobic/hydrophilic) shell structures that act as "all-in-one" smart nanomaterials is presented. The particles possess hydrophilic cores consisting of silica and a polyelectrolyte (PE) network and an amphiprotic shell consisting of superhydrophobic long-chained hydrocarbons and hydrophilic PEs. Due to the unique hydrophilic cores and amphiprotic shells, the particles exhibit extraordinary performance in terms of amphiprotic catalytic reactions in organic and aqueous solutions, oil/water separation and pollutant purification, and an ultrahigh loading capacity of enzymes with significant stability and efficient recyclability. The amphiprotic functionalities of the SHSMs have the potential to allow for a rich range of applications to be explored.

1. Introduction

Oil/water separation and micellar catalysts that utilize the hydrophilic/hydrophobic interface have consistently attracted attention for a long time. Due to the increasing requirements for environmental and water remediation, the selective separation of oil spills (or organic solvents) from water using polymer membranes/febrics,[1,2] metal meshes,[3,4] and sponges[5,6] has been the subject of extensive research in recent years. There are several methods for fabricating oil/water separation materials.[1–3,5–9] These methods include the fabrication of surfaces with superhydrophobicity and superoleophilicity for the separation of oil from water. However, these methods cannot remove/purify soluble pollutants in water. Most efforts have been devoted to separating oil from water and have not focused on pollutants in water. Very little attention has been focused on the purification of water-soluble pollutants after oil/water separation.[4] Thus, there is considerable interest in developing novel and facile methods for the simultaneous separation of oil from water and purification of water-soluble pollutants.

The practical application of organic micelle catalysts that utilize hydrophilic/hydrophobic interfaces has been limited by several disadvantages. For example, the stability of organic micelles depends on many parameters, such as the solvent polarity, critical micelle concentration, and reaction conditions, such as pH, water/oil ratio, and temperature.[10,11] Due to the narrow range of stability of organic micelles, the synthesis of inorganic micelles that have hydrophilic/hydrophobic interfaces, large surface areas, high porosities, tunable surfaces, and high recyclability has recently attracted some attention.[12,13] For example, Lin and co-workers reported a simple route to hierarchically assembling micelles and inorganic nanoparticles.[14] Yang and co-workers prepared functionalized mesoporous silica spheres consisting of a hydrophobic core and a hydrophilic micellar shell.[15] As a first example, Alivisatos and co-workers recently reported resin templates based on the synthesis of inorganic micelles with a hydrophilic cavity and a hydrophobic surface and its application as a catalyst in the bromination of alcohol.[16] There is still considerable interest in developing novel methods for the exploration of interior/exterior-functionalized, superhydrophobic, and nanostructured inorganic micelles. To fulfill the requirements of oil/water separation and inorganic micellar catalysis mentioned above, the development of hierarchical nanomaterials that have a hydrophilic interior and superhydrophobic/hydrophilic (amphiprotic) exterior is highly desirable, offering significant potential for multiple applications. To the best of our knowledge, this report is the first example of the synthesis of nanomaterials that have a hydrophilic core and amphiprotic shell for multiple applications, such as amphiprotic catalytic reactions, oil/water separation and pollutant purification, and enzyme immobilization with significant stability and efficient recyclability.

Herein, we present the preparation and multiple applications of superhydrophobic hollow SiO_2 micelles (SHSMs) with hydrophilic cores and amphiprotic (superhydrophobic/hydrophilic) shell structures that act as "all-in-one" smart nanomaterials. Our SHSMs are better than hydrophilic@hydrophobic micelles prepared using previously reported methods for several reasons: (i) the polyallylamine hydrochloride (PAH) chains were extended and survived from the core to the shell even

Dr. Md. S. Islam, S. H. Kim, Dr. O. H. Han, Dr. H.-J. Lee
Western Seoul Center
Korea Basic Science Institute (KBSI)
Seoul 03759, South Korea
E-mail: hajinlee@kbsi.re.kr
Prof. W. S. Choi
Department of Chemical and Biological Engineering
Hanbat National University
Daejeon 34158, South Korea
E-mail: choiws@hanbat.ac.kr
S. H. Kim
Department of Chemistry
Kyungpook National University
Daegu 41566, South Korea
Prof. O. H. Han, Prof. H.-J. Lee
Department of Chemistry and Nano Sciences
Ewah Womans University
Seoul 03760, South Korea

DOI: 10.1002/adfm.201502693

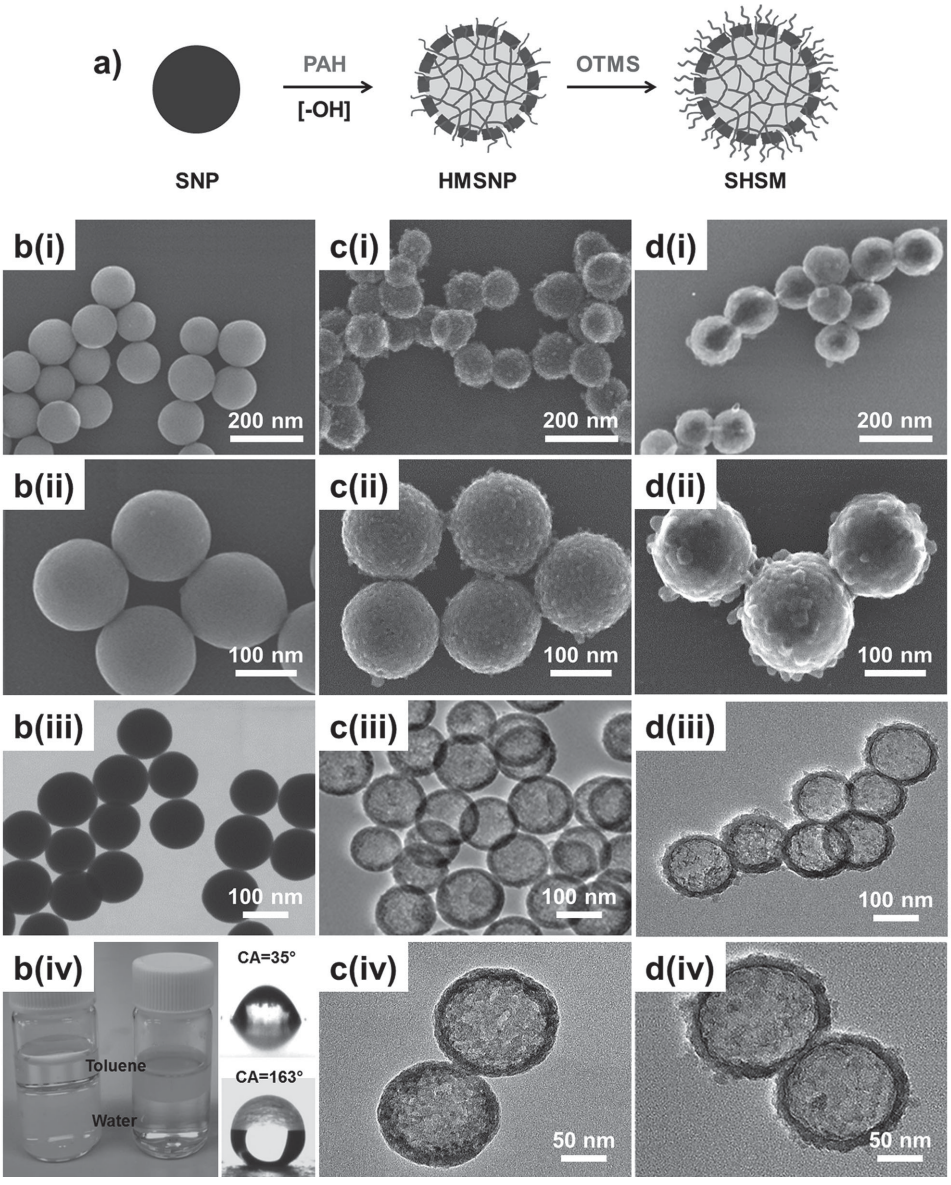

Figure 1. a) Schematic representation of the synthesis of the SHSMs. b–d) SEM and TEM images of each step in the formation of the SHSMs. b-i–iii) SEM and TEM images of the SNPs, b-iv) images of the HMSNPs dispersed in water and the SHSMs dispersed in toluene and their water contact angles (top: HMSNP and bottom: SHSM). c-i–iv) SEM and TEM images of the HMSNPs. d-i–iv) SEM and TEM images of the SHSMs.

after octadecyltrimethoxysilane (OTMS) treatment, meaning that hydrophilic groups (PAH) exist inside and outside of the SHSMs. In other words, hydrophilic PAH coexists with hydrophobic OTMS outside of the SHSMs. (ii) The SHSMs simultaneously showed hydrophilic (surface charge, +31.27 mV) as well as hydrophobic (superhydrophobicity, CA = 163°) properties due to their unique structures consisting of hydrophilic cores and amphiprotic shells. Therefore, amphiprotic shells and active amine groups made the SHSMs to use as catalysts for hydrophilic and hydrophobic environments. We demonstrate multiple applications of SHSMs: (a) inorganic catalysts for micelle catalytic reactions in organic or aqueous solutions, (b) superhydrophobic coating of sponges or metal meshes for oil/water separation and pollutant purification, and (c) hydrophobic carriers for ultrahigh loading of enzymes with significant stability and efficient recyclability.

2. Results and Discussion

Figure 1a shows a schematic illustration of the synthesis of SHSMs, which were prepared from hollow mesoporous SiO_2 nanoparticles (HMSNPs). The HMSNPs were synthesized via modification of our previously reported method.[17] By simply adding PAH to SiO_2 NPs (SNPs) solution, under high pH conditions (pH = 12) the NH_3^+ groups of the PAH become fully deprotonated to form the NH_2 groups. Therefore, PAH forms H-bond networks between PAH and PAH chains as well as

between PAH chains and the SNPs. The massive and heavy PAH networks, reinforced by a significant number of H-bonds, alter the balance of the SiO_2 network conformation and promote the cleavage of primary covalent bonds (Si–O–Si). Under high-pH conditions, PAH favors its neutral entangled form because of the reduced fraction of protonated amines. Thus, PAH is able to penetrate the SNP cores while the entangled PAH randomly or nonuniformly etch the SNPs due to decreased H-bond and charge interactions. Finally, the reaction between the SNPs and the PAH under alkaline conditions results in the formation of HMSNPs that are decorated with an interpenetrating PAH network inside and outside the hollow structures. After hydrophobization, long-chain hydrocarbons (OTMS) are covalently grafted onto the outer shell of the HMSNPs. Based on their silane chemistry, only the outer surfaces of hollow SNP shells could be modified by the hydrophobic OTMS.[18–20] The ultimate results are the formation of SHSMs with hydrophilic cores (due to the PAH) and amphiprotic shells (due to the PAH and OTMS) because the interpenetrating PAH coexists with the OTMS on the outer shell.

Figure 1b–d shows scanning electron microscopy (SEM) and transmission electron microscopy (TEM) images of each step of the formation of the SHSMs. Before the formation of the SHSMs, the SNPs showed a smooth surface morphology with a high density (Figure 1b). However, after the addition of PAH with sonication treatment, the surface morphology became rough, and HMSNPs with an average size of 140 nm (shell thickness: 14 nm) were observed (Figure 1c). What clearly distinguishes this method from our previously reported method is the importance of sonication. The internal and external structures of the HMSNPs remained unchanged. However, the surface charges of the HMSNPs were remarkably different from each other. The surface charge of the HMSNPs prepared using sonication was ζ = 32.84 mV, which was greater than the value (ζ = −10.17 mV) obtained from previously reported stirring method (without sonication) (Figure S1a–c, Supporting Information). Etching of SiO_2 using PAH can be activated via sonication because sonication remarkably reduces the reaction time (see the Experimental Section). As a result, the reaction progressed further using sonication, which led to a high charge density distribution of PAH at the surface of the HMSNPs prepared by sonication treatment. The resulting hydrophilic HMSNPs were used as a template for coating the OTMS, through which the hollow particle diameter (shell thickness) increased to 150 nm (19 nm) and the surface morphology became slightly smoother (Figure 1d). The static water contact angle (WCA) increased from 35° to 163°, and the hydrophilic HMSNPs successfully transformed into SHSMs, which were transferred from water to toluene after the OTMS coating (Figure 1b-iv). The Brunauer–Emmett–Teller (BET) specific surface area, Barrett–Joyner–Halenda (BJH) pore size, and pore volume of the HMSNPs were 196 m^2 g^{-1}, 14.3 nm, and 1.1 cm^3 g^{-1}, respectively, (Figure S2a, Supporting Information). For the SHSMs, these values decreased slightly to 155 m^2 g^{-1}, 11.2 nm, and 0.99 cm^3 g^{-1}, respectively, but the SHSMs still showed a typical type IV mesoporous structure even after coating with OTMS.

The coexistence of the PAH and the OTMS on the outer shell of the SHSMs was confirmed using Fourier transform infrared (FT-IR) spectroscopy, X-ray photoelectron spectroscopy (XPS), and zeta-potential measurements. The peaks at ≈1612 cm^{-1} and 2855–2920 cm^{-1} reveal the existence of amine groups (PAH,δ(N–H)) and alkyl chain groups (OTMS, $(C–H)_n$), respectively (Figure S2b, Supporting Information).[21] The XPS data confirmed the existence of amine groups (N1s) in the outer shell even after coating OTMS on the HMSNPs (Figure S3a, Supporting Information). Moreover, after the OTMS coating, the peak intensity of the C1s increased remarkably compared to that of the HMSNPs before the OTMS coating, indicating that the long alkyl chain of the OTMS was successfully grafted onto the surface of the HMSNPs. In the deconvoluted XPS spectrum of the N1s region, the peak below 400 eV corresponds to the nitrogen atoms involved in the formation of $–H_2N\cdots O$ (for SNP-PAH), $–NH\cdots O$ (for SNP-PAH), or $C{=}NH\cdots HN–$ (for PAH-PAH) bonds (Figure S3b, Supporting Information).[17] Another weak peak above 401.0 eV is attributed to protonated amine groups (NH_3^+). The surface charge of the SHSMs after the OTMS coating was ζ = 31.3 mV, which was similar to that of the HMSNPs (ζ = 32.8 mV) before the OTMS coating (Figure S1c, d, Supporting Information). The OTMS coating on the PAH-coated SNPs changed the surface charge of the PAH-coated SNPs from positive to negative, meaning that the positive charges of the PAH were screened by the OTMS, and thus, the negative charges of the SNPs were exposed (Figure S1e,f, Supporting Information). However, the charges of the PAH in the HMSNPs were not affected by OTMS because of the relatively vertically aligned, interpenetrating PAH, compared to the horizontally coated PAH on SNPs. The above-mentioned results suggest that the hydrophilic amine groups (PAH) could survive even after the OTMS coating and coexisted with the OTMS in the outer shell of the SHSMs. Furthermore, electron tomography images of the HMSNPs in Figure S4 (Supporting Information) show that the density of PAH inside the HMSNPs was higher than that of PAH outside the HMSNPs due to the formation of a cobweb-like internal structure consisting of PAH and SiO_2. As a result, the hydrophobic OTMS was observed to prefer silanization reactions in the outer shell of the HMSNPs.

Further investigation for the existence of PAH in both core and shell region of SHSMs was performed by solid-state magic angle spinning nuclear magnetic resonance (MAS NMR) analysis. **Figure 2**a_1–a_3 are ^{13}C MAS NMR spectra of PAH, HMSNPs and SHSMs, respectively. The resonance peaks at (i) 42–48 ppm and (ii) 26–40 ppm for HMSNPs are attributed to the C atoms bonded to N atom in NH_2 group of PAH and bonded to C atoms in alkyl groups of PAH, respectively (Figure 2a_1,a_2). Signals of PAH were observed in SHSMs, indicating the existence of PAH even after attachment of OTMS on HMSNPs (Figure 2a_3). Characteristic peaks around 0–40 ppm in Figure 2a_3 are attributed to C atoms in long alkyl chains of OTMS (1–18). According to the calculation using peak area data of deconvoluted ^{13}C MAS NMR spectra of SHSMs (Figure 2a_3), 30% and 70% of total carbons are occupied by PAH and OTMS, respectively. ^{29}Si MAS NMR spectra were obtained for quantitative analyses of Si-environments in various SNPs. The ^{29}Si MAS NMR spectra of all SNPs in Figure 2b_1–b_3 show Q bands. The signals at –87, –99, and –109 ppm are attributed to Q^2 [$Si(OH)_2(OSi)_2$, magenta lines], Q^3 [$Si(OH)(OSi)_3$, cyan lines], and Q^4 [$Si(OSi)_4$, black lines] silicon, respectively. The strong

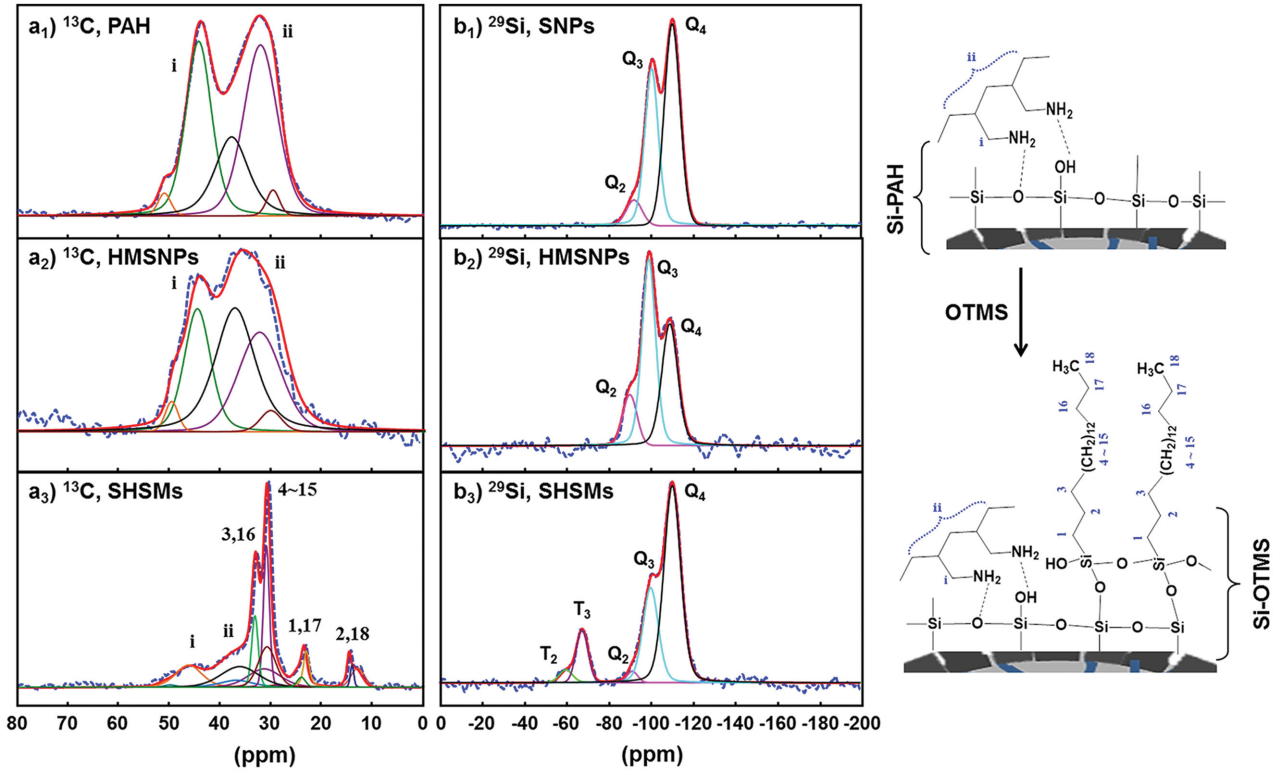

Figure 2. a) Solid-state ^{13}C MAS NMR spectra of a_1) PAH, a_2) HMSNPs, and a_3) SHSMs. b) Solid-state ^{29}Si MAS NMR spectra of b_1) SNPs, b_2) HMSNPs, and b_3) SHSMs. The blue dashed lines correspond to the experimental signals while the red solid lines correspond to the signal obtained by integration of all deconvoluted peaks represented by orange, green, black, purple, brown, cyan, and magenta lines. c) The schematics for possible interaction of PAH and OTMS on HMSNPs.

signals for higher order Q bands confirm that the solid material is subjected to a high degree of condensation.[15,22] SHSMs show T bands at –57 ppm for T^2 [$SiC(OH)(OSi)_2$, green line] and –66.8 for T^3 [$SiC(OSi)_3$, purple line] (Figure 2b_3). The presence of T bands confirms that organic moieties from OTMS are integrated with the HMSNPs through Si–C linkages in the shell region of SHSMs. Coverage of OTMS on the surface of SHSMs was calculated using peak area data of deconvoluted ^{29}Si MAS NMR spectra of SHSMs and HMSNPs as shown in Figure 2b_2,b_3. According to the calculation, 62 ± 2% of the total Si sites located in the inner and outer surfaces of HMSNPs contains hydroxyl groups (Si–OH), and 70 ± 3% of the total Si–OH sites located in HMSNPs exists on the outer surface of HMSNPs. When OTMS was coated on HMSNPs, 75 ± 3% of the hydroxyl groups on the outer surface of HMSNPs is chemically bonded to OTMS on the assumption that OTMS exists only on the outer surface of SHSMs. This means that on the outer surface of SHSMs hydrophilic silanol groups accounting for 25 ± 3% of hydroxyl groups on the outer surface of HMSNPs still remain, which can be occupied by the extended PAH chains. These results suggest amphiprotic nature of SHSMs shell.

To investigate the feasibility of using SHSMs as amphiprotic catalysts, AuNP-loaded SHSMs (SHSM–AuNPs) were prepared by synthesizing AuNPs within the HMSNPs, followed by treatment with OTMS (Figure S5, Supporting Information). **Figure 3**a shows TEM and STEM images of the SHSM–AuNPs. AuNPs (2 nm) were well distributed within the SHSMs. AuNPs were also observed in the outer shell (insets of Figure 3a), meaning that the AuNPs can be synthesized inside and outside the SHSMs due to the PAH inside as well as outside the SHSMs. The SHSMs formed a white suspension, but the suspension turned a wine color due to the formation of AuNPs (inset of Figure 2a-ii). The shapes of the absorption curves of the AuNPs were essentially the same in both cases, indicating that the properties of the Au catalysts did not change during the OTMS coating (Figure S5a, Supporting Information). In order to test for the diffusability of any hydrophilic reagent through the amphiprotic shell of SHSMs, or SHSM–AuNPs, the SHSM–AuNPs were used as nanocatalysts for the catalytic conversion of 4-nitrophenol (4-NPh) to 4-aminophenol (4-APh) in aqueous solution. Figure 3b and Figure S5b–d (Supporting Information) show the relationship between $\ln(C_t/C_0)$ and the reaction time (t) of the catalysts with various contents of OTMS. The OTMS content used for the hydrophobic coating is denoted by subscripts. All of these plots obey first-order reaction kinetics very well. The reaction constant (k = 0.66 min^{-1}) and the turnover frequency (TOF = 9143 h^{-1}) of the SHSM–$AuNP_{(0.5)}$ catalysts (CA = 135°) were lower than those of the hydrophilic HMSNP–AuNP catalysts (k = 1.3 min^{-1}, TOF = 21 395 h^{-1}) (Figure S5e, Supporting Information) because of the low diffusion rates of hydrophilic reagents (e.g., NPh and $NaBH_4$) through the mesoporous shell of the $SHSMs_{(0.5)}$. To verify this result, a more hydrophobic catalyst, i.e., SHSM–$AuNPs_{(1.0)}$

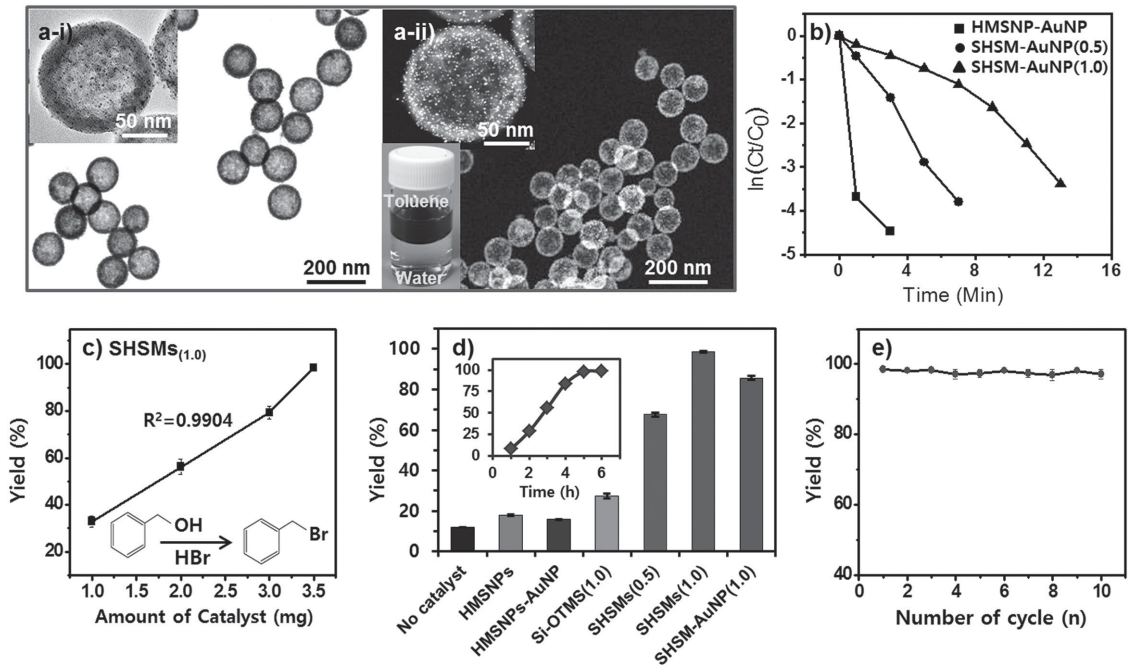

Figure 3. a-i) TEM and a-ii) STEM images of AuNP-loaded SHSMs (SHSM–AuNPs). The lower inset of (a-ii) shows the SHSM–AuNPs transferred from water to toluene after coating OTMS on the HMSNP–AuNPs. b) Plot of $\ln(C_t/C_0)$ versus the reaction time t for the reduction of 4-NPh by $NaBH_4$ in the presence of different catalysts. The OTMS content used for hydrophobic coating is denoted by subscripts. The yields of benzyl bromide converted from benzyl alcohol using HBr with the assistance of c) various amounts of the $SHSMs_{(1.0)}$ catalyst and d) different types of catalysts. The inset shows the progress of bromination as a function of the reaction time. The yields were calculated from ^1H NMR data. e) The reusability test for the conversion of benzyl alcohol over ten successive bromination cycles using $SHSMs_{(1.0)}$.

(CA = 152°), was used for the test. A lower reaction constant ($k = 0.36\ min^{-1}$) and TOF ($4952\ h^{-1}$) than those of the HMSNP–AuNPs and the SHSM–$AuNPs_{(0.5)}$ were obtained. The catalytic reactions were completed within 3, 7, and 13 min for the HMSNP–AuNPs, SHSM–$AuNPs_{(0.5)}$, and SHSM–$AuNPs_{(1.0)}$, respectively (Figure S5b–d, Supporting Information). These results indicate that the accessibility of the reactants through the shell of the SHSMs could be adjusted by controlling the hydrophobicity of the SHSMs, which is not easy in the case of organic micelles.[16] Although the diffusion of hydrophilic species through the SHSMs structure was much slower, its inner cavity still retained considerably higher accessibility for hydrophilic reactants. For example, even though the SHSM–$AuNPs_{(1.0)}$ possessed a higher proportion of hydrophobic moieties, they could completely transform the NPh into APh within 13 min due to the hydrophilic PAH interpenetrated along the core and into the shell (Figure 3b and Figure S5d, Supporting Information). The interpenetrated PAH served as a medium that helped hydrophilic reagents diffuse inside the SHSMs. In the case of normal SNP–$AuNPs_{(1.0)}$ (SNP/PAH/AuNP/OTMS), only 7% of the NPh was transformed, and the reaction was not complete even after 12 h due to the very low diffusion rate of the hydrophilic reagents (Figure S6, Supporting Information). These results suggest that the reaction activity of the SHSM–$AuNPs_{(1.0)}$ in aqueous solution could be maintained by interpenetrating PAH even after coating with OTMS.

To investigate the aforementioned catalytic reactions in organic solvents, we also tested the SHSMs for organic synthesis reactions. The bromination of primary alcohols was selected as a model reaction. Figure 2c shows tunable yields of benzyl bromide converted from benzyl alcohol using various amounts of the $SHSMs_{(1.0)}$ catalyst. The optimum reaction conditions, i.e., the catalyst amount and time, were observed to be 3.5 mg and 6 h, respectively (Figure 3c,d). Without any catalyst, only 12% of the benzyl alcohol was converted to benzyl bromide (Figure 3d). In the presence of $SHSMs_{(1.0)}$ or SHSM–$AuNPs_{(1.0)}$, the yields dramatically increased to 98% and 86%, respectively. In the case of the $SHSMs_{(0.5)}$, the conversion rate was 68%. The performances were better at higher proportions of the hydrophobic moieties. Additional tests were performed using various types of catalysts. To investigate the effect of the mesoporous structures of the $SHSMs_{(1.0)}$, we used entirely hydrophobic (CA = 152°) OTMS-treated SNPs (Si-OTMS) as a catalyst. Their yield was only 27%. The above mentioned results indicate that high proportions of hydrophobic moieties as well as micellar structures are indispensable for efficient catalytic bromination reactions of alcohol with a high yield. The reusability of the $SHSMs_{(1.0)}$ was also tested (Figure 3e). The productivity of the $SHSMs_{(1.0)}$ remained nearly almost unchanged after ten cycles, which could be very promising for practical applications in other organic synthesis reactions.

A major challenge remains in developing scalable methodologies that enable superhydrophobic coatings on versatile substrates with a combination of strong stability, high efficiency for industrial applications, and great reusability. Therefore, our second application was focused on the environmental remediation issues such as oil/water separation and pollutant purification. They were performed using both the SHSMs and

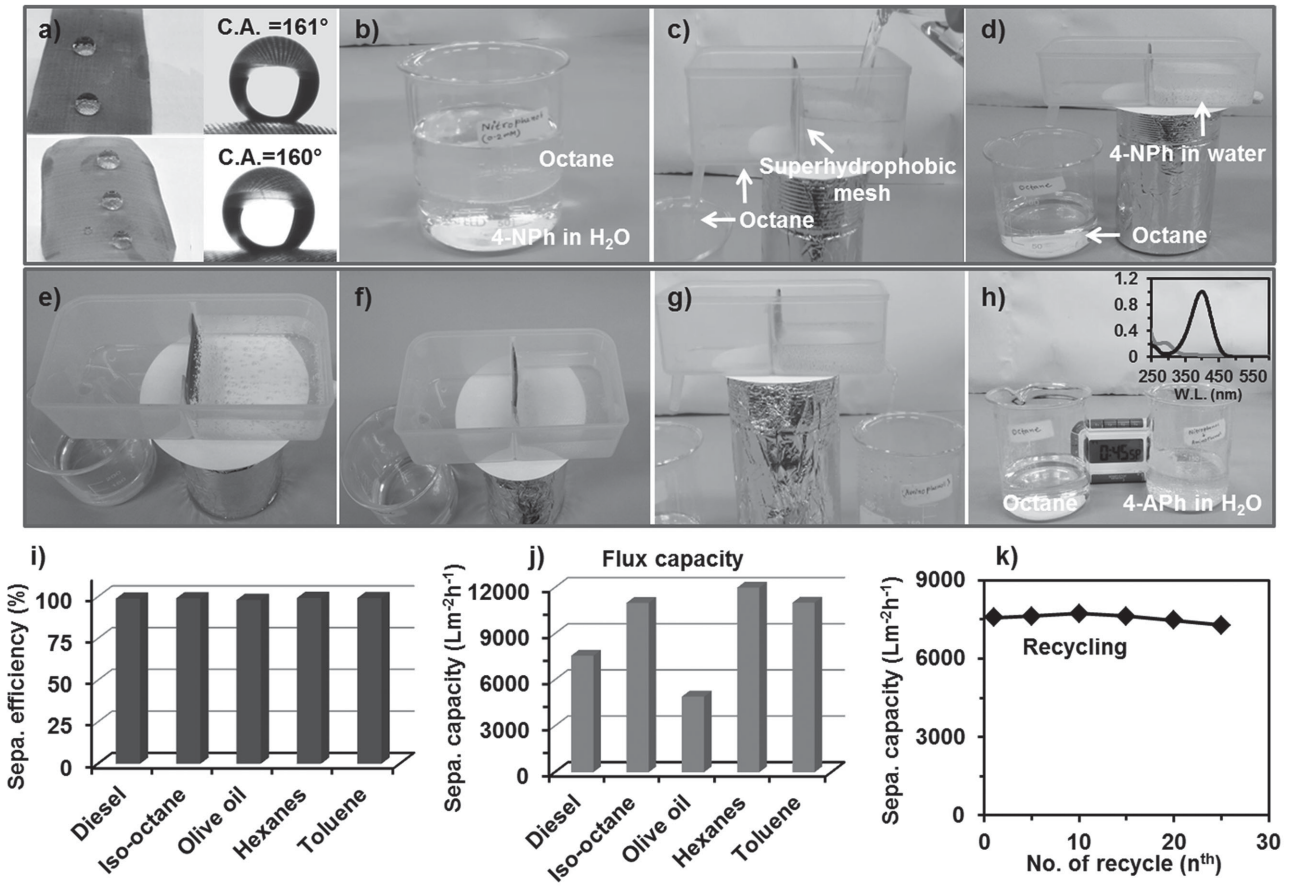

Figure 4. a) Images of the SHSM–AuNP-coated Cu (upper) and stainless steel (lower) meshes and their water contact angles. b–h) Images showing the purification process of the pollutant (4-NPh) in water during the oil/water separation using the SHSM–AuNPs$_{(1.0)}$-coated stainless steel mesh. b) Image of mixed solutions of oil (octane) and water (4-NPh). c,d) Images of octane emitted through the drain and 4-NPh remaining in the right compartment. e–h) Images showing the separation process of octane and 4-APh (left one) formed via purification of 4-NPh (right one). The inset of (h) shows the transformation of 4-NPh (black line) into 4-APh (gray line) caused by contact between 4-NPh and the SHSM–AuNP-coated stainless steel mesh. i) Separation efficiencies and j) capacities (flux) of various types of oils. k) Reusability test for diesel oil over 25 consecutive cycles using the SHSM–AuNPs$_{(1.0)}$-coated stainless steel mesh.

SHSM–AuNPs$_{(1.0)}$. Cleaning up oil spills, oil slicks, and hydrophobic organic reagents from water surfaces is an important issue in environmental and ecological safety. We fabricated catalyst-loaded superhydrophobic meshes with multiple functions that involve oil separation and aqueous contaminant removal from water. Two types of superhydrophobic metal mesh filters (Cu or stainless steel, CA > 160°) were prepared by dip coating the meshes in SHSM–AuNPs$_{(1.0)}$ solutions. **Figure 4**a shows photographs of the copper and stainless steel meshes after coating the SHSM–AuNPs$_{(1.0)}$. The SHSM–AuNPs$_{(1.0)}$-coated meshes exhibited a water CA of over 160° and an oil (diesel) CA of 0°. This superhydrophobicity remained stable for a long time, even for a month. The deposition of the SHSM–AuNPs$_{(1.0)}$ on the surface of both types of metal meshes was confirmed by SEM measurements (Figure S7, Supporting Information). The SHSM–AuNPs$_{(1.0)}$ were tightly bound to negatively charged meshes due to the positively charged PAH coexisting with OTMS in the shell of the SHSMs (Figure S1, Supporting Information). Figure 4b–h shows the simultaneous separation of oil and removal of aqueous contaminants from the water. A plastic chamber equipped with a catalyst-coated superhydrophobic mesh was used for the rapid filtration of oils or hydrophobic solvents. After the addition of a mixture of oil/water (Octane/4-NPh in water), only the oil could quickly be separated at a very high flux rate (Figure 4c,d). The time required to remove 100 mL of oil ranged from 60 s for octane to a maximum of 135 s for olive oil, based on the oil's density. However, water (colored with 4-NPh) could not pass through the mesh (Figure 4d,e). The 4-NPhs were gradually transformed into 4-APhs when the 4-NPh solution was held within the right compartment (Figure 4f). After 45 min, the yellow 4-NPh solution became a transparent 4-APh solution, which was collected (Figure 4e–g). To summarize, the oil was completely separated from contaminated water using the SHSM–AuNPs$_{(1.0)}$-coated mesh with a superhydrophobic component (OTMS), and simultaneously, the contaminated water was completely purified via contact with the SHSM–AuNPs$_{(1.0)}$-coated mesh possessing a hydrophilic component (PAH–AuNPs) (Figure 4h). The SHSM–AuNPs$_{(1.0)}$ with hydrophilic cores and amphiprotic shells showed multiple functions, such as oil/water separation and aqueous contaminant removal, which are not observed in normal oil/water separation materials with only superhydrophobic

components. Photographs illustrating oil/water separation of various types of oils can be found in Figure S8 (Supporting Information). Moreover, the separation efficiencies of oils reached 99.3% and 99.1% for stainless steel and Cu meshes, respectively (Figure 4i and Figure S7c, Supporting Information). The calculated maximum separation capacities (flux) of the stainless steel and Cu meshes were 12 036 L m^{-2} h^{-1} for hexane and 11 016 L m^{-2} h^{-1} for toluene, respectively (Figure 4j and Figure S7d, Supporting Information), which exhibited much higher flux rates compared than those reported in other studies.[23–26] Both types of SHSM–$AuNP_{(1.0)}$-coated meshes showed nearly constant recyclabilities for diesel oil over 25 consecutive cycles (Figure 4k and Figure S7e, Supporting Information). These results indicate that the SHSM–$AuNP_{(1.0)}$-coated mesh filters could be very promising for large-scale applications in industrial sectors in which high separation efficiency, great recyclability, and low cost are very important.

As an extension of the study of oil/water separation, SHSM-coated superhydrophobic sponges were prepared, which exhibited excellent absorption capacities for oil and organic solvents from water mixtures, with high selectivities and extraordinary recyclabilities. A commercially available melamine-formaldehyde sulfate (MF) sponge was used and coated with the SHSMs using the dip coating method mentioned above. **Figure 5**a–d shows photographs and SEM images of the MF sponge before and after hydrophobization. The sponge showed a hydrophilic nature and smooth surface morphology before hydrophobization (Figure 5a,b). After coating the SHSMs, the sponge floated on water without sinking (Figure 5c). The surface was dramatically transformed from a wetting into a superhydrophobic surface (CA = 165°). The sponge showed a rough surface morphology because it was coated with the SHSMs (Figure 5d). The SHSMs were tightly bound to the negatively charged sponge surface due to the coexistence of positively charged PAH and OTMS in the shell of the SHSMs.

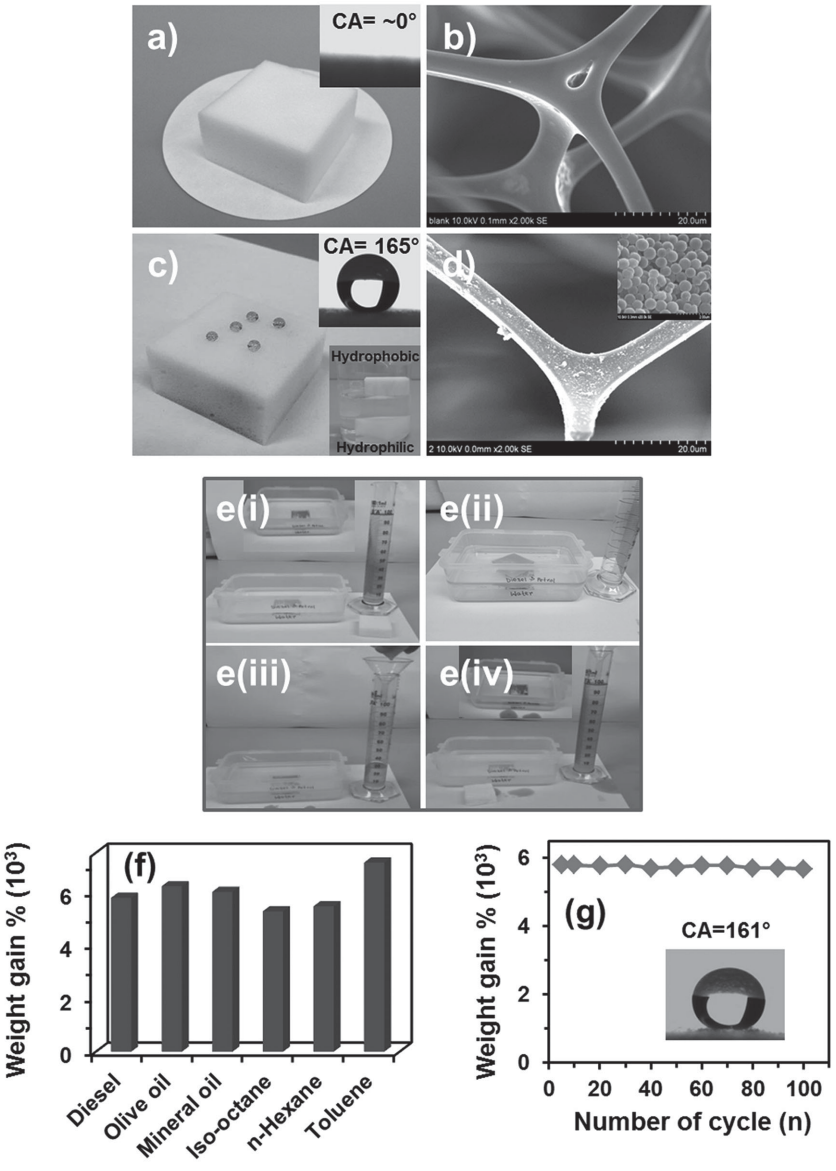

Figure 5. Photographic and SEM images of the MF sponge a,b) before and c,d) after coating with the SHSMs. a,c) Insets showing their water contact angles. c) Inset showing a sinking and floating MF sponge before and after coating with the SHSMs, respectively. d) Inset showing enlarged image of the SHSMs immobilized on the sponge surface. e-i–iv) Images showing the oil absorption, separation, and recycling process from the oil/water mixture. f) Absorption capacities for various oils. g) Reusability test for diesel oil absorption over 100 consecutive cycles using the superhydrophobic sponges ($SHSMs_{(1.0)}$-coated MF sponge). The inset of (g) shows static CA of a superhydrophobic sponge after the 100th cycle.

The sponge's potential for practical application, such as in oil absorption from oil/water mixtures, was tested by placing a piece of the SHSM-coated MF sponge ($4 \times 4 \times 2$ cm^3) on a mixture of various oils. Figure 5e and Figure S9 (Supporting Information) show that the extent of oil separation reached 99% from oil/water mixtures via absorption and squeezing. In addition, the superhydrophobic sponge exhibited excellent absorption capacities toward a wide range of oils and organic solvents, up to 58–71 times the sponge's own weight (Figure 5f and Figure S10, Supporting Information). The calculated absorption capacities were 629–772 kg m^{-3} (Figure S10, Supporting Information). The superhydrophobic sponges also showed excellent recyclability with high sorption capacity retention (>97%, CA = 161°) and mechanical stability after 100 cycles of sorption-squeezing of diesel oils (Figure 4g and Figure S11, Supporting Information). These results suggest that superhydrophobic sponges with excellent absorption capacities, recyclabilities, and mechanical stabilities offer significant technological abilities in the fields of water remediation, clean up of oil spills, and oil recovery.

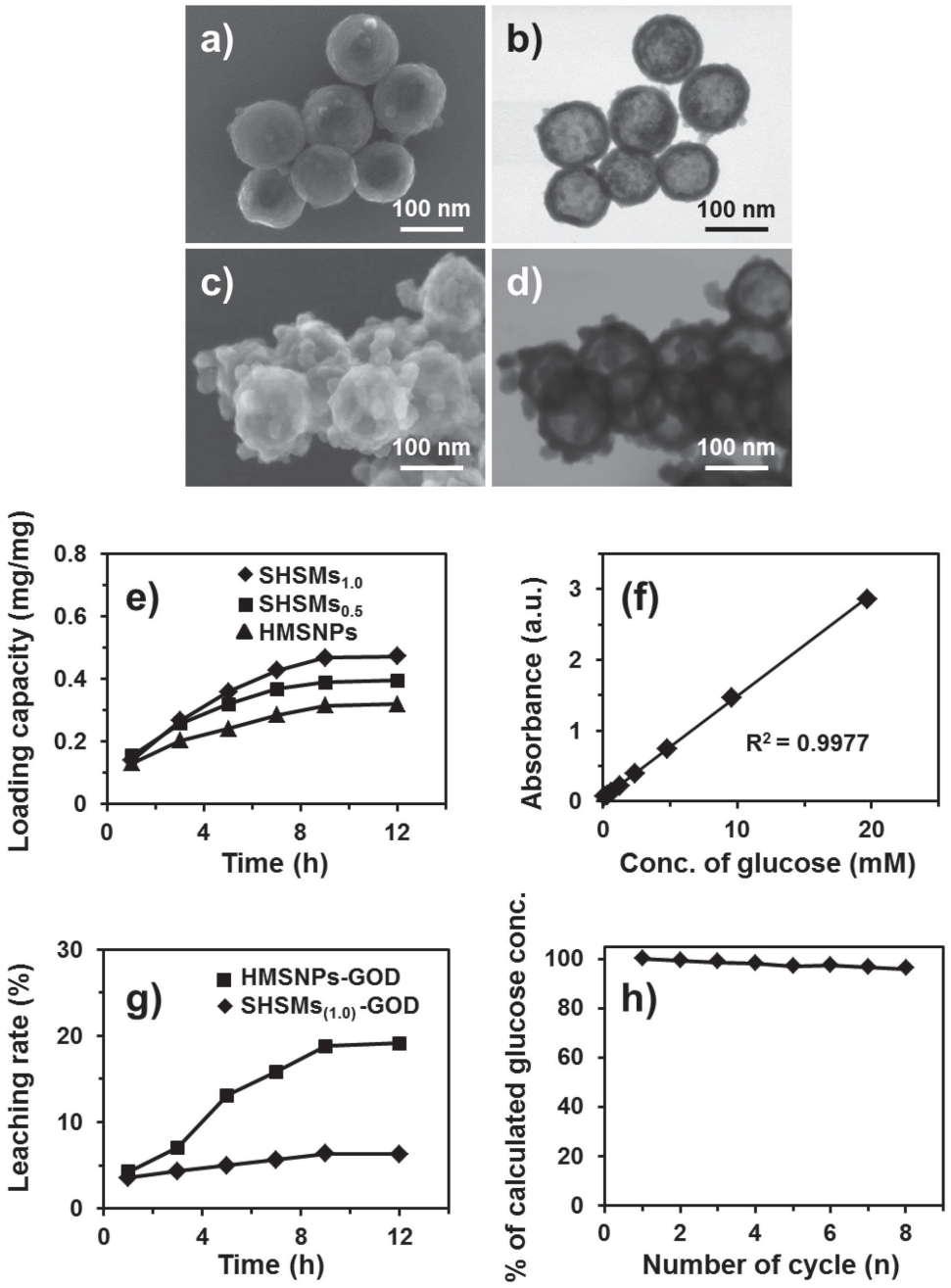

Figure 6. a,c) SEM and b,d) TEM images of GOD-immobilized carriers. a,b) hydrophilic HMSNPs–GOD and c,d) $SHSMs_{(1.0)}$–GOD. e) Comparative loading capacities of GOD using HMSNPs, $SHSMs_{(0.5)}$, and $SHSMs_{(1.0)}$. f) Representative data for the activity of GOD in the $SHSMs_{(1.0)}$–GOD for glucose oxidation. g) Desorption or leaching profile of GOD from the HMSNPs–GOD and the $SHSMs_{(1.0)}$-GOD in sodium acetate buffer (pH = 4.0) over 12 h. h) Reusability test over eight consecutive cycles with the $SHSM_{(1.0)}$-GOD.

Finally, to investigate the potential application of the SHSMs as supporters for bulky molecules, such as glucose oxidase (GOD), the extensively used enzyme was tested as a model enzyme. Hydrophilic carriers often show limited loading capacities, a lack of long-term stability under operating conditions, and difficulties in recovery and recycling. To overcome these limitations, the development of hydrophobic carriers with an ultrahigh loading of GOD, significant stability, and efficient recyclability is challenging. Therefore, the GOD loading capacity of the SHSMs was evaluated by mixing GOD (0.8 mg mL^{-1}) and three types of carriers (i.e., HMSNPs, $SHSMs_{(0.5)}$, and $SHSMs_{(1.0)}$). The hydrophilic HMSNPs showed a relatively smooth surface after loading GOD, whereas the $SHSMs_{(1.0)}$ showed a bumpy surface morphology (**Figure 6**a–d). After loading GOD, the BET surface area and pore size of $SHSM_{(1.0)}$–GOD decreased to 25% (43.7 m^2 g^{-1})

and 30% (3.3 nm) those of the pristine $SHSMs_{(1.0)}$, respectively (Figure S12a, Supporting Information). The calculated loading of GOD onto the hydrophilic HMSNPs was 0.318 mg mg^{-1}, whereas the calculated GOD loading amounts were 0.395 and 0.473 mg for the $SHSMs_{(0.5)}$ and $SHSMs_{(1.0)}$, respectively (Figure 6e and Figure S13, Supporting Information). These values are significantly higher than those indicated in previous reports.[27] GOD could interact with the hydrophilic HMSNPs through a nonelectrostatic interactions, such as van der Waals interactions and hydrogen bonding. In contrast, due to the superhydrophobic nature of the SHSMs, large amounts GOD could interact with the SHSMs' long alkyl chains through hydrophobic interactions, which are relatively stronger than other weak intermolecular forces, such as van der Waals interactions or hydrogen bonding.[28] With increasing amounts of OTMS, the GOD loading capacity of the $SHSMs_{(1.0)}$ exceeded that of the $SHSMs_{(0.5)}$, which was 1.5 times higher than that of the hydrophilic HMSNPs (Figure 6e and Figure S13, Supporting Information). The activity of GOD immobilized on the SHSMs was investigated using Fenton's assay and the rate of iron oxidation due to hydrogen peroxide production.[29] Because GOD catalyzes the oxidation of glucose to D-gluconic acid and hydrogen peroxide, the activity of GOD could be determined by measuring the amount of hydrogen peroxide formed. The determination of an unknown glucose concentration can be divided into two steps. In this study, a standard calibration curve (linear equation, $Y = 0.2897x + 0.0467$) was first obtained via the reaction between H_2O_2 with various concentrations ($0.062–5 \times 10^{-3}$ M) and Fenton`s reagent (Figure S12b–d, Supporting Information). Then, a glucose solution with a known concentration ($0.152–20 \times 10^{-3}$ M) was added to a mixture of Fenton's reagent and $SHSM_{(1.0)}$–GOD. The glucose oxidized using GOD produced H_2O_2, which then oxidized Fenton's reagent; the latter process was monitored at 334 nm using a spectrophotometer (Figure S14a, Supporting Information). Finally, the concentration of glucose was calculated by substituting the UV absorbance values (at 334 nm) into the above-mentioned linear equation. For accuracy (%), the actual and calculated concentrations of glucose were compared (Figure S14c, Supporting Information). Figure 6f and Figure S14c (Supporting Information) demonstrate the excellent accuracy (95%–98%) attained using $SHSM_{(1.0)}$–GOD for the detection of glucose. The R^2 value (0.9977) indicates good accuracy for the glucose calculated using the corresponding standard equation. These results suggest that the SHSMs could be utilized as carriers for high loading amounts of GOD and for the determination of unknown glucose concentrations in various biological and nonbiological samples. The mechanical stability of immobilized GOD was checked for hydrophilic HMSNP–GOD and $SHSM_{(1.0)}$–GOD after the dispersion of each sample in sodium acetate buffer. Figure 6g and Figure S14b (Supporting Information) show that the leaching of GOD increased over time. $SHSM_{(1.0)}$–GOD showed very high mechanical stability and a low desorption rate (≈6%) for GOD, whereas the hydrophilic HMSNP–GOD showed a dispersion rate of 19% because hydrophobic interactions are stronger than van der Waals interactions or hydrogen bonding as mentioned above.[28] $SHSM_{(1.0)}$–GOD showed excellent reusability after eight cycles (Figure 6h). Only 4% of the activity of $SHSM_{(1.0)}$–GOD was lost. The above-described results indicate that SHSM could be used as a novel supporter while maintaining high bioactivity and low leaching of enzymes.

3. Conclusion

In conclusion, we demonstrated the preparation and multiple applications of SHSMs with hydrophilic cores and amphiprotic (superhydrophobic/hydrophilic) shells. The unique amphiprotic functionality made the SHSMs suitable as smart nanomaterials for multiple applications, such as amphiprotic catalytic reactions in aqueous or organic solutions, oil/water separation and pollutant purification, and enzyme immobilization with great stability and efficient recyclability. The SHSM–AuNPs and the SHSMs showed excellent catalytic activity toward the reduction of nitrophenol and catalyzing bromination of alcohols, respectively. Amphiprotic functional groups enabled the SHSMs to tightly attach themselves to sponges or meshes to prepare superhydrophobic sponges with excellent absorption performances and extraordinary recyclabilities and superhydrophobic meshes with extremely high flux rates. It was also possible to purify water-soluble pollutants during the oil/water separation. Moreover, the SHSMs exhibited ultrahigh enzyme loading capacities and high stability and recyclability. We believe that due to the unique hydrophilic cores and amphiprotic shells, the SHSMs offer significant technological promises in the fields of water remediation, clean up of oil spills, oil recovery, biosensing, drug delivery, and controlled release.

4. Experimental Section

Materials: Tetraethyl orthosilicate (TEOS, 99.99%), poly(allylamine hydrochloride) (PAH, M_w = 58 kD), sodium borohydride ($NaBH_4$), ethyl alcohol (99.99%), ammonium hydroxide solution (28%–30%), hydrobromic acid (HBr, 48% solution), benzyl alcohol (>99.0%), anhydrous toluene (>99.8%), hexamethylbenzene (99%), chloroauric acid ($HAuCl_4$, 99.99%), anhydrous 1,2-dichlorobenzene (DCB, 99%), dichloromethane, *n*-octadecyltrimethoxysilane (OTMS, 99%), iron (II) sulfate ($FeSO_4{\cdot}7H_2O$, 99%), D-(+)-glucose (99%), glucose oxidase from Aspergillus niger (176 000 units g^{-1}), and mineral oil (heavy metal white) were purchased from Sigma-Aldrich. Granular sodium hydroxide and iso-octane (99.4%) were purchased from Showa Chemicals Co. Ltd. All chemicals were used without further purification. Diesel oil, olive oil, nylon sponges, and MF sponges were purchased from a local market, and 200-mesh copper and stainless steel screens were obtained from TWP Inc. Berkeley, CA, USA.

Synthesis of Hollow Mesoporous Silica Nanoparticles (HMSNPs): TEOS (0.8 mL) was added to a mixture of deionized water (2 mL) and ethyl alcohol (8 mL) and stirred for 10 min. An ammonium hydroxide solution (0.1 mL) was added to the mixture and continuously stirred for 6 h. The resulting milky white SNP solution was then washed with ethanol and used in the following steps. The SNPs (0.1 g) were dispersed in ethyl alcohol (2 mL) in a bath-type sonicator. Then, 10 mL of PAH (2 mg mL^{-1}, pH = 9.0) was added dropwise to the SNPs solution and continuously sonicated for 30 min. Finally, an aqueous sodium hydroxide solution (1.5 mL, 0.3 M) was added and sonicated for another 10 min. Reaction time required for synthesis of HMSNPs was dramatically decreased from 24 h to 40 min by using sonication, compared with previous method.[14] The product was washed with ethyl alcohol and water three times and redispersed in 10 mL of ethanol.

Synthesis of AuNP-Loaded HMSNPs (HMSNP–AuNPs): An aqueous $HAuCl_4$ solution (5×10^{-3} M, 1 mL) was injected into an ethanol solution of HMSNPs (10 mL) and stirred for 30 min. The $HAuCl_4$ was then reduced via the addition of an aqueous $NaBH_4$ solution (5×10^{-3} M, 0.05 mL). The resulting HMSNP–AuNPs were collected by washing with copious amounts of water and ethanol.

Synthesis of Superhydrophobic Hollow Silica Micelles (SHSMs or SHSM–AuNPs): 1 mL of *n*-OTMS was added dropwise to 20 mL of a 1,2-dichlorobenzene (DCB) solution containing 0.1 g of HMSNPs or HMSNP-AuNPs and stirred for 30 min. Then, the solution was degassed for 10 min under argon gas bubbling and heated to 150 °C in a furnace for 3 h to introduce hydrophobic carbon chains onto the surface of the HMSNPs or HMSNP–AuNPs. After cooling to room temperature, the modified materials were washed with toluene and ethanol several times. The resulting materials were denoted $SHSMs_{(1.0)}$, $SHSMs_{(0.5)}$, or $SHSMs_{(0.25)}$ depending on the volume of OTMS added (e.g., 1, 0.5, or 0.25 mL, respectively) per 0.1 g of HMSNPs.

Detailed information for catalytic tests, oil/water separation tests, enzyme immobilization, and characterization can be found in the Supporting Information.

Supporting Information

Supporting Information is available from the Wiley Online Library or from the author.

Acknowledgements

This research was supported by the Korea Basic Science Institute (grant T35740), the Basic Science Research Program of the National Research Foundation of Korea (NRF) funded by the Ministry of Science, ICT & Future Planning (2014003515), and the National Research Council of Science and Technology through the Degree & Research Center program (DRC-14-3-KBSI).

Received: July 1, 2015
Revised: August 4, 2015
Published online: September 1, 2015

[1] Z. Xu, Y. Zhao, H. Wang, X. Wang, T. Lin, *Angew. Chem. Int. Ed.* **2015**, *54*, 1452.
[2] W. Zhang, Z. Shi, F. Zhang, X. Liu, J. Jin, L. Jiang, *Adv. Mater.* **2013**, *25*, 2071.
[3] Y. Wang, Y. Shi, L. Pan, M. Yang, L. Peng, S. Zong, Y. Shi, G. Yu, *Nano Lett.* **2014**, *14*, 4803.
[4] C. Gao, Z. Sun, K. Li, Y. Chen, Y. Cao, S. Zhang, L. Feng, *Energy Environ. Sci.* **2013**, *6*, 1147.
[5] C. Ruan, K. Ai, X. Li, L. Lu, *Angew. Chem. Int. Ed.* **2014**, *53*, 5556.
[6] V. H. Pham, J. H. Dickerson, *ACS Appl. Mater. Interfaces* **2014**, *6*, 14181.
[7] H. Bi, Z. Yin, X. Cao, X. Xie, C. Tan, X. Huang, B. Chen, F. Chen, Q. Yang, X. Bu, X. Lu, L. Sun, H. Zhang, *Adv. Mater.* **2013**, *25*, 5916.
[8] D. D. Nguyen, N.-H. Tai, S.-B. Lee, W.-S. Kuo, *Energy Environ. Sci.* **2012**, *5*, 7908.
[9] G. Hayase, K. Kanamori, M. Fukuchi, H. Kaji, K. Nakanishi, *Angew. Chem. Int. Ed.* **2013**, *52*, 1986.
[10] W. O. Yah, A. Takahara, Y. M. Lvov, *J. Am. Chem. Soc.* **2012**, *134*, 1853.
[11] W. Meier, *Chem. Soc. Rev.* **2000**, *29*, 295.
[12] A. Abbaspourrad, N. J. Carroll, S. H. Kim, D. A. Weitz, *Adv. Mater.* **2013**, *25*, 3215.
[13] F. X. Liang, J. G. Liu, C. L. Zhang, X. Z. Qu, J. L. Li, Z. Z. Yang, *Chem. Commun.* **2011**, *47*, 1231.
[14] W. Han, M. Byun, B. Li, X. Pang, Z. Lin, *Angew. Chem. Int. Ed.* **2012**, *51*, 12588.
[15] S. Li, X. Jiao, H. Yang, *Langmuir* **2013**, *29*, 1228.
[16] Q. Zhang, X. Z. Shu, J. M. Lucas, F. D. Toste, G. A. Somorjai, A. P. Alivisatos, *Nano Lett.* **2014**, *14*, 379.
[17] Md. S. Islam, W. S. Choi, H. J. Lee, *ACS Appl. Mater. Interfaces* **2014**, *6*, 9563.
[18] A. N. Parikh, D. L. Allara, I. B. Azouz, F. Rondelez, *J. Phys. Chem.* **1994**, *98*, 7577.
[19] J. B. Brzoska, I. B. Azouz, F. Rondelez, *Langmuir* **1994**, *10*, 4367.
[20] N. Garcia, E. Benito, J. Guzman, P. Tiemblo, *J. Am. Chem. Soc.* **2007**, *129*, 5052.
[21] S. Yang, D. Chen, N. Li, X. Mei, X. Qi, H. Li, Q. Xu, J. J. Lu, *Mater. Chem.* **2012**, *22*, 25354.
[22] L. Fu, S. Li, Z. Han, H. Liu, H. Yang, *Chem. Commun.* **2014**, *50*, 10045.
[23] W. Zhang, Z. Shi, F. Zhang, X. Liu, J. Jin, L. Jiang, *Adv. Mater.* **2013**, *25*, 2071.
[24] X. Deng, L. Mammen, H. J. Butt, D. Vollmer, *Science* **2012**, *335*, 67.
[25] X. Deng, L. Mammen, Y. Zhao, P. Lellig, K. Müllen, C. Li, H. J. Butt, D. Vollmer, *Adv. Mater.* **2011**, *23*, 2962.
[26] Y. Wang, Y. Shi, L. Pan, M. Yang, L. Peng, S. Zong, Y. Shi, G. Yu, *Nano Lett.* **2014**, *14*, 4803.
[27] S. Cao, B. Liu, *Macromol. Biosci.* **2009**, *9*, 361.
[28] R. H. Garrett, C. M. Grisham, *Biochemistry*, 3rd ed, Thomas Brooks/Cole, Belmont, CA **2005**, p. 15.
[29] A. Subramanian, S. J. Kennel, P. I. Oden, K. B. Jacobson, J. Woodward, M. J. Doktycz, *Enzyme Microb. Technol.* **1999**, *24*, 26.